Journal of Superconductivity and Novel Magnetism (2025) 38:5
https://doi.org/10.1007/s10948-024-06887-3

BRIEF REPORT

# A $^{151}$Eu Mössbauer investigation of Magnetic Ordering in the Topological Material Candidate $EuZnBi_2$

**D. H. Ryan**[1]

Received: 26 June 2024 / Accepted: 4 September 2024


**Abstract**
Recently, Junbao He et al. reported on magnetic ordering in the topological candidate $EuZnBi_2$ (He et al. J. Supercond. Nov. Magn. **37**, 579 2024) and suggested that there is a spin reorientation near 15 K, below the initial antiferromagnetic transition at $T_N$=20 K. Here we use $^{151}$Eu Mössbauer spectroscopy to show that the situation is more complex. The initial ordering involves an incommensurate sinusoidally modulated structure that progressively squares up on further cooling.

**Keywords** Mössbauer spectroscopy · Magnetic ordering · Topological material · Europium compound

## 1 Introduction

The tetragonal $ATX_2$ compound family provides a rich variety of systems in which to search for interesting magnetic behaviour. When grown with X = Sb or Bi, both the A and T sites can host either a magnetic (A = Eu, Yb; B = Mn) or non-magnetic (A = Ca, Sr; B = Zn) species allowing for three distinct magnetic configurations, and a fourth non-magnetic configuration. The crystal structure is formed by stacking alternating layers of square-planar ($X^-$) two-dimensional (2D) Dirac conduction layers and magnetic insulating layers ($A^{2+}$–$B^{2+}$–$X^{3-}$) [2]. $EuMnBi_2$ has been studied extensively, particularly for the impact of the europium ordering on the 2D Dirac fermion behaviour within the square-planar bismuth layer [3–6]. By contrast, the isostructural and potentially simpler $EuZnBi_2$ appears to have been ignored. Recently, Junbao He et al. [1] reported a bulk characterisation of $EuZnBi_2$. Their results suggested an easy-plane antiferromagnetic (AF) structure at 3 K with a magnetisation that fell far short of the expected 7 $\mu_B$/Eu in 7 Tesla. However, the Curie-Weiss susceptibility gave an effective europium moment of 8.00$\mu_B$(ab) and 8.05$\mu_B$(c) consistent with the 7.94$\mu_B$/Eu expected for fully divalent europium. The Néel temperature was reported as 20 K. All of these results are essentially identical to those found for $EuZnSb_2$ [7, 8].

It is their additional suggestion that a spin reorientation transition occurs at $T_{sr}$=15 K that is the focus of the current work. Both dc and ac susceptibility showed evidence for a second event below $T_N$ in $EuZnBi_2$ [1] that could be suppressed by a dc field of about 0.5 T. Although the susceptibility signatures are clear, heat capacity only shows the peak due to AF ordering at 20 K with no additional anomaly. Here, we use $^{151}$Eu Mössbauer spectroscopy to investigate the valence and ordering behaviour of the europium in $EuZnBi_2$. We find that the europium is fully divalent and confirm $T_N$=20K. However, we also find that the initial ordering at $T_N$ is to an incommensurate sinusoidally modulated structure and not to a simple ab-plane AF state. Further cooling leads to the modulation becoming square-wave. It is not possible to determine whether this square-wave order is commensurate or remains incommensurate solely on the basis of Mössbauer data. Diffraction measurements, using either x-rays or neutrons, are needed to make that determination. See, for example, $EuIn_2$ where a similar sinusoidal to square-wave evolution of the order was observed and x-ray resonant magnetic scattering (XRMS) measurements showed that the ordering remained incommensurate [9].

## 2 Experimental Methods

The single-crystal growth sequence used here was based on that previously described by He et al. [1]. A starting

✉ D. H. Ryan
dhryan@physics.mcgill.ca

[1] Physics Department and Centre for the Physics of Materials, McGill University, 3600 University Street, Montreal, QC H3A 2T8, Canada

Published online: 13 December 2024

composition of $EuZn_5Bi_{10}$ (Eu ingot, 99.9% Thermo Fisher Scientific; Zn shot, 99.9999% and Bi ingot 99.999% Alfa-Aesar) was loaded into a fritted alumina Canfield crucible set (CCS) [10, 11] and sealed into a fused silica tube with a partial pressure of helium for thermal exchange. The sample was heated to 900°C over 10 h, held for 5 h to form a homogeneous liquid, and then decanted by centrifuging at 900°C [12]. This step removes any high melting point materials (typically oxide contaminants) that could provide nucleation sites leading to small crystals. These solid impurities can also make it more difficult to collect clean crystals as they remain in the growth crucible along with the target material. The collected liquid fraction was re-loaded into a sealed fused silica tube with a fresh frit and catch crucible. It was remelted by heating to 900°C over 5 h, held for 5 h, then slow-cooled to 450°C over 160 h and finally decanted to recover the crystals.

Faceted 5×5 mm-sized flat crystals were obtained, and phase identity was confirmed by Cu-$K_\alpha$ powder x-ray diffraction. X-ray diffraction measurements were made on a Bruker Phaser-II diffractometer using a Cu-$K_\alpha$ source. Rietveld refinement of the powder diffraction pattern was carried out using the GSAS/EXPGUI packages [13, 14]. The fitted lattice parameters given below are consistent with the previous report [1].

$^{151}$Eu Mössbauer spectroscopy measurements were carried out on a conventional spectrometer driven in sinusoidal mode and calibrated using a standard $^{57}$CoRh/$\alpha$-Fe foil. Isomer shifts are quoted relative to $EuF_3$ at ambient temperature. A thin (0.25 inch) NaI(Tl) scintillation detector was employed to detect the transmitted gammas. ~120 mg of $EuZnBi_2$ was hand-ground in an agate mortar under hexane to protect from oxidation. The mass chosen was a compromise between making the sample thick enough to yield a useful signal but not so thick as to reduce the transmitted intensity too much. Bismuth is a high-Z element and as such, it strongly absorbs the 21.6 keV gammas used for $^{151}$Eu Mössbauer spectroscopy. The spectra presented here were each collected for 4–5 days. The powder was mixed with boron nitride to make a uniform absorber and loaded into a thin-window Delrin holder. The sample was cooled in a vibration-isolated closed-cycle helium refrigerator with the sample in helium exchange gas. The simpler spectra were fitted to a sum of Lorentzian lines with the positions and intensities derived from a full solution to the nuclear Hamiltonian [15]. In cases where an incommensurate modulated magnetic structure was observed, the spectra were fitted using a distribution of hyperfine fields ($B_{hf}$) derived from an (assumed) sinusoidal modulation of the moments [16, 17].

## 3 Results

### 3.1 X-ray Diffraction

$EuZnBi_2$ grew as thin (<1 mm) plates that were typically 5×5 mm in size (see inset to Fig. 1). The crystals appear to be air-stable on a timescale of months. Rietveld refinement of the x-ray diffraction pattern shown in Fig. 1 confirmed phase identity with residual bismuth being the only observed impurity (typically 10–15 wt.%). Assuming the I4/mmm (#139) space group and structure reported by He et al. [1], we obtain fitted lattice parameters of $a = b$ =4.6173(3) Å

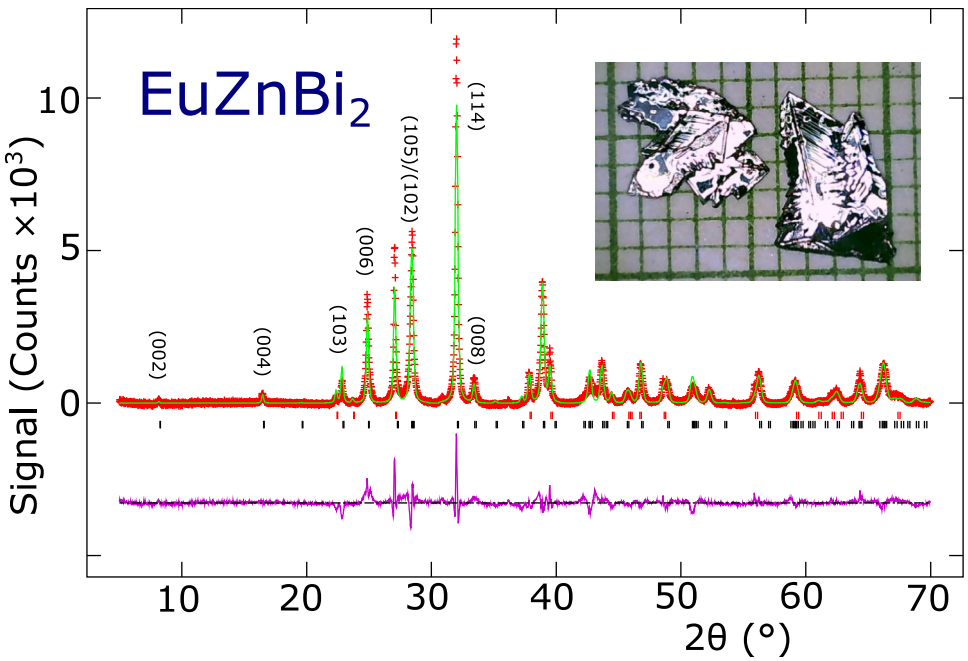


**Fig. 1** Powder x-ray diffraction pattern for $EuZnBi_2$ with the Rietveld refinement shown in green and the residuals shown below in purple. Bragg markers are for the ~15 wt.% residual bismuth flux (top row, red) and the primary $EuZnBi_2$ phase (bottom row, black). Indices for some of the lower angle diffraction peaks from $EuZnBi_2$ are given. The inset shows some typical crystals on mm graph paper

and $c$ =21.381(2) Å, consistent with the previous report [1]. The diffraction data are shown with the Rietveld fit in Fig. 1. Measurements on a single flake showed only the 0 0 2$l$ reflections indicating that the c-axis is perpendicular to the plates, as previously reported by He et al. [1].

### 3.2 $^{151}$Eu Mössbauer Spectroscopy

Several conclusions can easily be drawn from the $^{151}$Eu Mössbauer spectra of $EuZnBi_2$ shown in Fig. 2. At 25 K, in the paramagnetic state above $T_N$, we observe a single feature with an isomer shift of −11.63(4) mm/s typical of fully divalent europium [18] and a linewidth (HWHM) of 1.16(10) mm/s (the large uncertainty coming from fitting correlations with the small, ∼5 mm/s, quadrupole contribution). We do not observe any signal that could be associated with the presence of trivalent europium (<3%) so we conclude that all of the europium in $EuZnBi_2$ is present as $Eu^{2+}$ as in $EuZnSb_2$ [7, 8], $EuMnSb_2$ [19] and $EuMnBi_2$ [20]. At 4.8 K the magnetic order is well established and we observe a hyperfine field ($B_{hf}$) of 25.89(11) T, slightly smaller than the 27.0(1) T seen in $EuMnSb_2$ [19]. The linewidth of 1.20(5) mm/s shows minimal broadening. Thus, at 4.8 K the ordered magnetic structure of $EuZnBi_2$ involves a single unique europium environment, consistent with the AF order inferred by He et al. [1]. Finally, if we follow the temperature dependence of $B_{hf}$ shown in Fig. 3 and fit $B_{hf}(T)$ using a simple $J = \frac{7}{2}$ mean-field model appropriate for the $Eu^{2+}$ ion, we obtain a Néel temperature of $T_N$=19.9(1) K, fully consistent with He et al. [1].

Although our initial analysis appears to yield results that are consistent with the simple AF ordering at $T_N$ followed by a reorientation at $T_{sr}$ ∼15 K proposed by He et al. [1], closer examination yields several significant discrepancies. The position of the possible spin reorientation transition at $T_{sr}$ ∼15 K is marked on Fig. 3, however, we do not observe any change in the behaviour of $B_{hf}(T)$ in the vicinity of $T_{sr}$. More significantly, if we plot the linewidth derived from the single-site full Hamiltonian fits [15] in Fig. 4 we see that there is an abrupt increase on warming through ∼11 K. This increase in linewidth suggests the progressive development

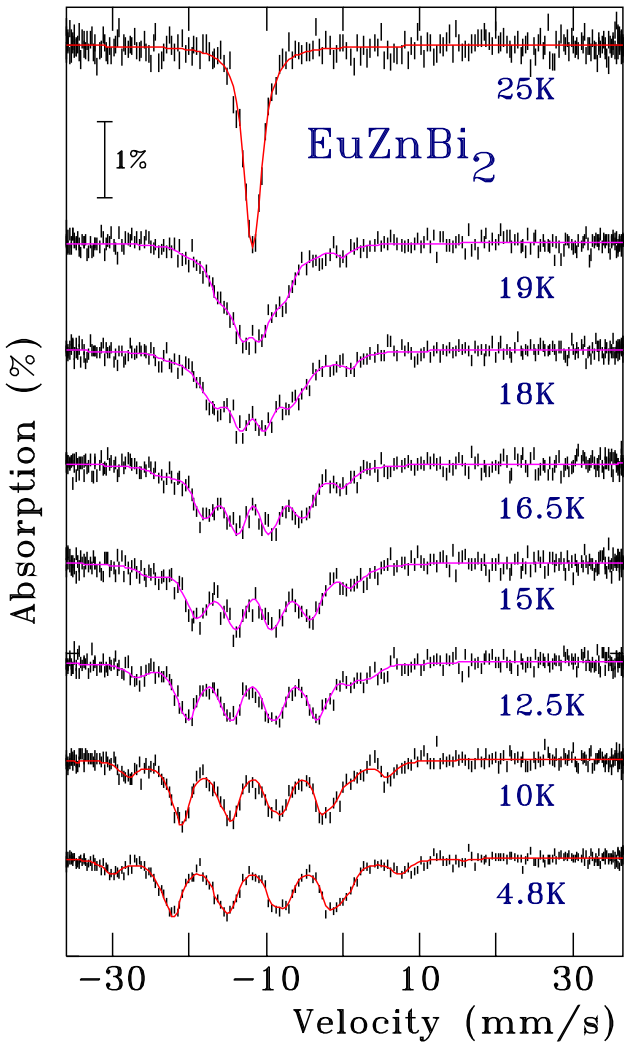


**Fig. 2** $^{151}$Eu Mössbauer spectra of $EuZnBi_2$ showing the evolution of the spectra with temperature. The lines clearly broaden on warming and the spectra develop a characteristic "droop" towards the centre. The solid red lines through the lowest and highest temperature spectra are fits derived from the full Hamiltonian solution, whereas the magenta lines through the remaining, intermediate temperature spectra are fits derived from the incommensurate modulation model (see text for details of both models)

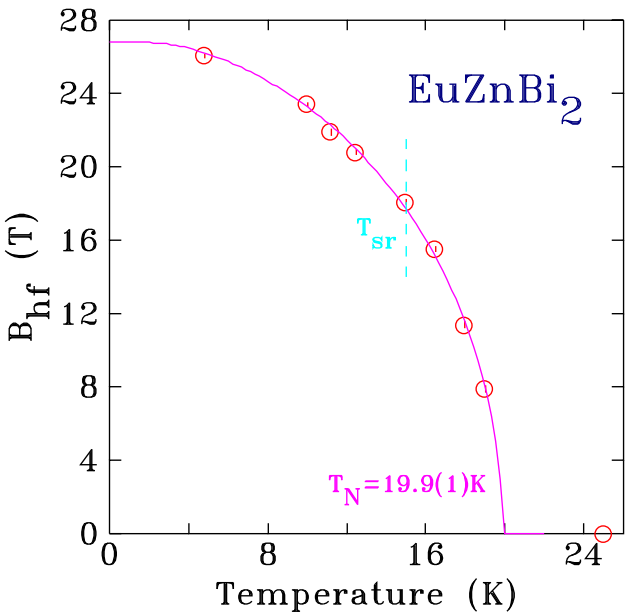


**Fig. 3** Temperature dependence of the hyperfine field ($B_{hf}$) for $EuZnBi_2$. The solid line is a fit using a simple $J = \frac{7}{2}$ mean-field model appropriate for the $Eu^{2+}$ ion. The dashed line at 15 K marks the position of the suggested spin reorientation temperature [1]

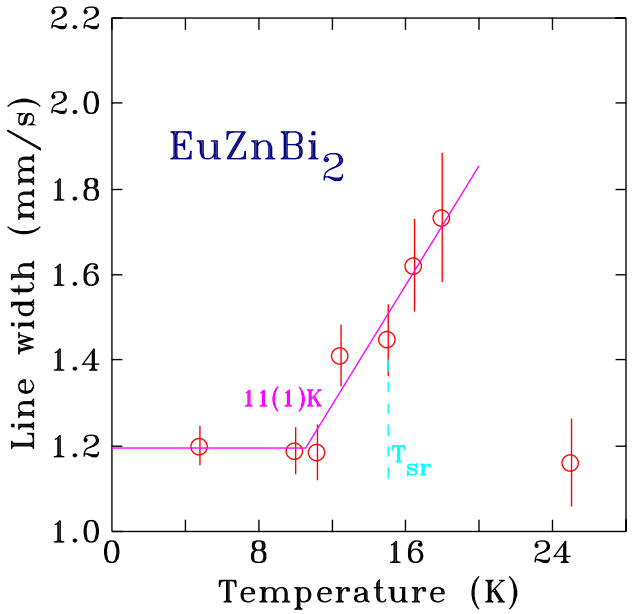


**Fig. 4** Evolution of the fitted linewidth for $EuZnBi_2$ using a single-site full Hamiltonian model to fit the spectra. Note the clear break near 11 K where the fitted linewidth starts to increase rapidly. The point at 25 K taken in the paramagnetic state confirms that the linewidth recovers once the magnetic contributions are absent

of a distribution in the europium moment magnitudes above 11 K. By contrast, a simple spin reorientation would only lead to a change in the projection of $\overrightarrow{B_{hf}}$ onto the principal axis of the electric field gradient ($\overrightarrow{V_{zz}}$) without causing any change in the observed linewidth. Furthermore, the quadrupole contribution observed in the paramagnetic state for $EuZnBi_2$ is too small for such a change to be easily fitted.

The evolution of the spectral shapes in Fig. 2 seen on warming through 11 K is more consistent with the development of an incommensurate modulated ordering of the europium moments. The four strongest lines in the spectra clearly broaden and the spectra overall develop a characteristic "droop" towards the centre, as the central doublet appears to extend below the lines to their immediate left and right (all four are normally approximately the same intensity, see for example the spectrum at 4.8 K). To fit these spectra, we assume that the moment modulation along the direction of the propagation vector **k** can be written in terms of its Fourier components, and further assume that the observed hyperfine field is a linear function of the magnitude of the Eu moment at any given site. The variation of $B_{hf}$ with distance $x$ along the propagation vector **k** can then be written as: [17]

$$B_{hf}(kx) = Bk_0 + \sum_{l=0}^{n} Bk_{2l+1} \sin[(2l+1)kx] \quad (1)$$

where the $Bk_n$ ($n = 2l+1$) are the odd Fourier coefficients of the field (moment) modulation. As $+B_{hf}$ and $-B_{hf}$ are indistinguishable, $kx$ only needs to run over half the modulation period, and in this case, a square-wave modulated structure can be modeled either as a sum over a very large number of Fourier coefficients, or by simply using the $Bk_0$ term with all of the other $Bk_n$ set to zero. We have found that fits are far more stable with the $Bk_0$ term included rather than using a large set of $Bk_n$, however, the two approaches are effectively equivalent. Variations of this model have also been used to fit spectra of EuPdSb [17], $Eu_4PdMg$ [21], $EuAl_4$ [22] and $EuIn_2$ [9].

The results of these modulated fits are shown as magenta lines in Fig. 2, while the full Hamiltonian fits at the high (paramagnetic) and low temperatures are shown as red lines. Plotting the various components derived from the fits *vs.* temperature in Fig. 5 provides some insights into the nature of the magnetic order in $EuZnBi_2$. Fitting the temperature dependence of the average hyperfine field ($B_{avg}$) to a J=$\frac{7}{2}$ mean-field model appropriate for $Eu^{2+}$ yields a transition temperature of 20.0(1) K consistent with our value derived from the full Hamiltonian fits earlier. Starting from above $T_N$ and cooling, we see that the first stages of the ordering are dominated by incommensurate contributions from $Bk_1$ and $Bk_3$, i.e. the initial ordering is to an incommensurate, sinusoidally modulated state. On cooling both terms grow and by about 16 K the modulation starts to become more square

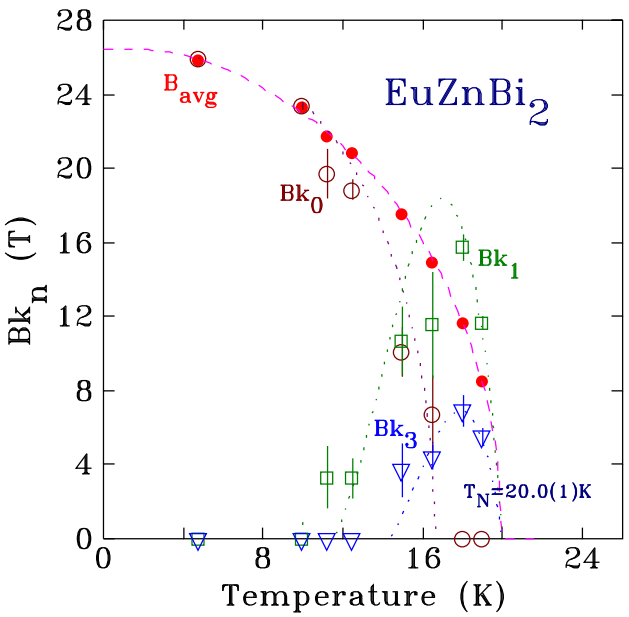


**Fig. 5** Temperature dependence of the average hyperfine field ($B_{avg}$) and three Fourier components ($Bk_0$, $Bk_1$ and $Bk_3$) for $EuZnBi_2$ derived from the incommensurate modulated model described in the text. Fitting a J=$\frac{7}{2}$ mean-field model through $B_{avg}$(T) yields a transition temperature of 20.0(1) K, consistent both with $T_N$=19.9(1) K derived from the full Hamiltonian fits shown in Fig. 3, and the 20 K reported by He et al. [1]. It is apparent that the rapid increase in linewidth shown in Fig. 4 on warming through 11 K is associated with the development of several Fourier components in the hyperfine field distribution (see text for more details)

as the $Bk_0$ term is needed. Further cooling leads to a decline in both $Bk_1$ and $Bk_3$ while $Bk_0$ becomes dominant. Below 11 K the order is now fully square-wave, the modulated contributions to the order are lost and a simple, single-site model with no hyperfine field distribution fits the spectra with reasonable linewidths. We emphasise that although a single-site model fits the lowest temperature spectra, this does not necessarily mean that the magnetic order is now *commensurate*. Any magnetic structure in which the europium ions all have the same moment *magnitude* will yield a simple, sharp spectrum, especially if the moment *directions* all make the same angle with respect to the principal axis of the local electric field gradient. This situation is clearly illustrated by $EuIn_2$ which follows a similar modulated (below 14 K) to squared-up (below 9 K) ordering path as the current $EuZnBi_2$, but x-ray resonant magnetic scattering (XRMS) shows that the order remains incommensurate down to at least 5 K [9]. Similar diffraction work would be needed to establish the detailed nature of the T=0 K ordered state in $EuZnBi_2$.

## 4 Conclusions

$^{151}$Eu Mössbauer spectroscopy shows that the magnetic ordering in $EuZnBi_2$ is more complex than the paramagnetic $\rightarrow AF(T_N) \rightarrow T_{sr}$ sequence proposed by He et al. [1]. We find that the initial ordering is to an incommensurate sinusoidally modulated state that squares up progressively on cooling to a fully square-wave state by 11 K. Diffraction measurements (using either neutrons or resonant x-rays) will be needed to determine the actual nature (commensurate or incommensurate) of the final ordered state.

**Acknowledgements** Financial support for this work was provided by Fonds Québécois de la Recherche sur la Nature et les Technologies, and the Natural Sciences and Engineering Research Council (NSERC) Canada.

**Author Contributions** D.H.R. made the sample, carried out the measurements and analysed the data.

**Data Availability** The data that support the findings of this study are available from the corresponding author upon reasonable request.

## Declarations

**Conflict of Interest** The author declares no competing interests.

## References

1. He, J., Liu, B., Ma, S., Jin, S., Zheng, C., Fu, Y., Zhu, W., Cheng, J., Liu, C., Li, L., Ji, X., Luo, Y., Shi, H.: J. Supercond. Nov. Magn. **37**, 579 (2024). https://doi.org/10.1007/s10948-024-06704-x
2. Lee, G., Farhan, M.A., Kim, J.S., Shim, J.H.: Phys. Rev. B **87**, 245104 (2013). https://doi.org/10.1103/PhysRevB.87.245104. https://link.aps.org/doi/10.1103/PhysRevB.87.245104
3. May, A.F., McGuire, M.A., Sales, B.C.: Phys. Rev. B **90**, 075109 (2014). https://link.aps.org/doi/10.1103/PhysRevB.90.075109
4. Masuda, H., Sakai, H., Tokunaga, M., Yamasaki, Y., Miyake, A., Shiogai, J., Nakamura, S., Awaji, S., Tsukazaki, A., Nakao, H., Murakami, Y., Arima, T., Tokura, Y., Ishiwata, S.: Sci. Adv. **2**, e1501117 (2016)
5. Masuda, H., Sakai, H., Tokunaga, M., Ochi, M., Takahashi, H., Akiba, K., Miyake, A., Kuroki, K., Tokura, Y., Ishiwata, S.: Phys. Rev. B **98**, 161108 (2018). https://doi.org/10.1103/PhysRevB.98.161108. https://link.aps.org/doi/10.1103/PhysRevB.98.161108
6. Shiomi, Y., Watanabe, H., Masuda, H., Takahashi, H., Yanase, Y., Ishiwata, S.: Phys. Rev. Lett. **122**, 127207 (2019). https://doi.org/10.1103/PhysRevLett.122.127207. https://link.aps.org/doi/10.1103/PhysRevLett.122.127207
7. Wang, A., Baranets, S., Liu, Y., Tong, X., Stavitski, E., Zhang, J., Chai, Y., Yin, W.G., Bobev, S., Petrovic, C.: Phys. Rev. Res. **2**, 033462 (2020). https://doi.org/10.1103/PhysRevResearch.2.033462. https://link.aps.org/doi/10.1103/PhysRevResearch.2.033462
8. Wang, A., Baranets, S., Liu, Y., Tong, X., Stavitski, E., Zhang, J., Chai, Y., Yin, W.G., Bobev, S., Petrovic, C.: Phys. Rev. Res. **3**, 029002 (2021). https://doi.org/10.1103/PhysRevResearch.3.029002. https://link.aps.org/doi/10.1103/PhysRevResearch.3.029002
9. Kuthanazhi, B., Riberolles, S.X.M., Ryan, D.H., Ryan, P.J., Kim, J.W., Wang, L.L., McQueeney, R.J., Ueland, B.G., Canfield, P.C.: Phys. Rev. B **109**, 214401 (2024)
10. Canfield, P.C., Kong, T., Kaluarachchi, U.S., Jo, N.H.: Philosophical Magazine **96**(1), 84 (2016)
11. LSP Industrial Ceramics, Inc. Canfield crucible sets. https://www.lspceramics.com/canfield-crucible-sets-2/ [Accessed: 11-Jun-2024]
12. Canfield, P.C.: Reports on progress in physics **83**(1), 016501 (2019). https://doi.org/10.1088/1361-6633/ab514b
13. Larson, A.C., Von Dreele, R.B.: Los Alamos national laboratory report LAUR 86–748 (2000)
14. Toby, B.H.: J. Appl. Cryst. **34**, 210 (2001)
15. Voyer, C.J., Ryan, D.H.: Hyperfine Interact. **170**, 91 (2006)
16. Maurya, A., Bonville, P., Thamizhavel, A., Dhar, S.K.: Journal of Physics: Condensed Matter **26**, 216001 (2014)
17. Bonville, P., Hodges, J.A., Shirakawa, M., Kasaya, M., Schmitt, D.: Eur. Phys. J. B **21**, 349 (2001)
18. Long, G.J., Grandjean, F. (eds.) Mössbauer spectroscopy applied to inorganic chemistry, *Modern Inorganic Chemistry*, vol. 3 (Plenum Press NY, 1989)
19. Wilde, J.M., Riberolles, S.X.M., Das, A., Liu, Y., Heitmann, T.W., Wang, X., Straszheim, W.E., Bud'ko, S.L., Canfield, P.C., Kreyssig, A., McQueeney, R.J., Ryan, D.H., Ueland, B.G.: Phys. Rev. B **106**, 024420 (2022). https://doi.org/10.1103/PhysRevB.106.024420. https://link.aps.org/doi/10.1103/PhysRevB.106.024420
20. Jose, G.C., Xie, W., Lavina, B., Zhao, J., Alp, E.E., Zhang, D., Bi, W.: J. Phys.: Condensed matter **36**(25), 255802 (2024). https://doi.org/10.1088/1361-648X/ad3473
21. Ryan, D.H., Legros, A., Niehaus, O., Pöttgen, R., Cadogan, J.M., Flacau, R.: J. Appl. Phys. **117**, 17D108 (2015)
22. Ryan, D.H., Kuthanazhi, B., Jo, N.H., Canfield, P.C.: AIP Advances **14**(1), 015239 (2024)